Recent Advances in High-Flux, Two-Phase Thermal Management

Issam Mudawar

Purdue University Boiling and Two-Phase
Flow Laboratory (PU-BTPFL) and International
Electronic Cooling Alliance (PU-IECA),
Mechanical Engineering Building,
585 Purdue Mall,
West Lafayette, IN 47907-2088

Recent developments in applications such as computer data centers, electric vehicle power electronics, avionics, radars, and lasers have led to alarming increases in heat dissipation rate, which now far exceeds the capability of air cooling schemes and even the most aggressive single-phase liquid cooling schemes. This trend is responsible for a recent transition to two-phase cooling, which capitalizes upon the coolant's latent heat rather than sensible heat alone to achieve several order-of-magnitude increases in heat transfer coefficient. Three two-phase cooling configurations have surfaced as best contenders for the most demanding applications: mini/microchannel, jet, and spray. This study will explore the implementation of these configurations into practical cooling packages, assess available predictive tools, and identify future research needs for each. It is shown that the design and performance assessment of high-flux, two-phase cooling systems are highly dependent on empirical or semiempirical predictive tools and, to a far lesser extent, theoretical mechanistic models. A major challenge in using such tools is the lack of databases for coolants with drastically different thermophysical properties, and which cover broad ranges of such important parameters as flow passage size, mass velocity, quality, and pressure. Recommendations are therefore made for future research to correct any critical knowledge gaps, including the need for robust computer algorithms. Also discussed is a new class of "hybrid" cooling schemes that capitalize upon the merits of multiple cooling configurations. It is shown that these hybrid schemes not only surpass the basic cooling configurations in heat dissipation rate, but they also provide better surface temperature uniformity. [DOI: 10.1115/1.4023599]

1 Introduction

High-Heat-Flux Applications and Cooling Solutions. The aggressive microminiaturization of electronic components that started in the early 1980s created an urgent need for innovative cooling schemes to maintain chip temperatures below limits set by both materials and device reliability. Initial efforts focused on fan-cooled heat sink attachments. But as heat dissipation rate continued to escalate, interest shifted to dielectric liquid coolants using a variety of single-phase cooling schemes. By the mid-1980s, advanced computer chips were projected to dissipate in excess of $100 \, \text{W/cm}^2$, a threshold that exceeded the capability of single-phase liquid cooling solutions [1]. Since single-phase cooling relies entirely on the coolant's sensible heat rise, cooling system developers began to explore two-phase solutions to take advantage of the coolant's combined sensible and latent heat to absorb far greater amounts heat than with single-phase systems while maintaining relatively low surface temperatures.

But heat dissipation challenges were not limited to computer chips. Since the early 1990s, similar challenges began to emerge with devices found in numerous medical, transportation, energy, aerospace, and defense applications [2] as shown in Fig. 1. These applications spurred intense new research efforts in pursuit of high performance two-phase cooling solutions using a variety of cooling configurations and surface enhancement techniques. Of these configurations, three have gained the most attention: mini/microchannel, jet, and spray.

Two-phase mini/microchannel heat sinks are ideally suited for applications demanding the dissipation of large amounts of heat within very limited space. These heat sinks are highly compact and lightweight and require a very small coolant inventory. They also provide very high heat transfer coefficients and good surface temperature uniformity when the coolant undergoes phase change along the channel. Jet impingement produces very high heat transfer coefficients in a concentrated region—stagnation zone—of the impacted surface; better surface temperature uniformity is achieved with multiple jets. Spray cooling offers the merits of high heat transfer coefficients and moderate surface temperature uniformity. Aside from the mentioned attributes of mini/microchannel, jet, and spray cooling schemes, each offers unique advantages compared to the other two but also suffers important disadvantages.

Before addressing these issues for the individual configurations, it is important to first examine the most pressing challenge to the development of two-phase cooling solutions: the lack of accurate, universal predictive tools.

Challenges in Predicting Performance of Two-Phase Cooling Systems. Accurate predictive tools are essential to designing a cooling system for a high-heat-flux application using a mini/microchannel, jet, or spray configuration. To design such a cooling system and/or predict cooling performance, thermal engineers rely mostly on empirical correlations that are derived from databases for different coolants, geometrical parameters, and operating conditions. However, unlike single-phase correlations, two-phase correlations often provide inaccurate predictions. The following comparison provides a compelling reason for this important shortcoming.

Consider the popular Dittus–Boelter equation for turbulent fluid flow in a heated tube [3],

$$\text{Nu} = \frac{hD}{k_f} = 0.023 \text{Re}^{0.8} \text{Pr}^{0.4} \quad \begin{cases} \text{Re} > 10,000 \\ 0.6 < \text{Pr} < 160 \end{cases} \quad (1)$$

The effectiveness of this correlation is the result of both its reliance on appropriate dimensionless groups and broad application range. It consists of a single dimensionless group, Nu, that is a function of only two dependent dimensionless groups, Re and Pr. With a Reynolds number range of $\text{Re} > 10,000$, this correlation covers very broad ranges of flow rates and fluid properties. And excepting liquid metals and highly viscous fluids, the Prandtl number range of 0.6–160 covers many types of fluids, including both liquids and gases.
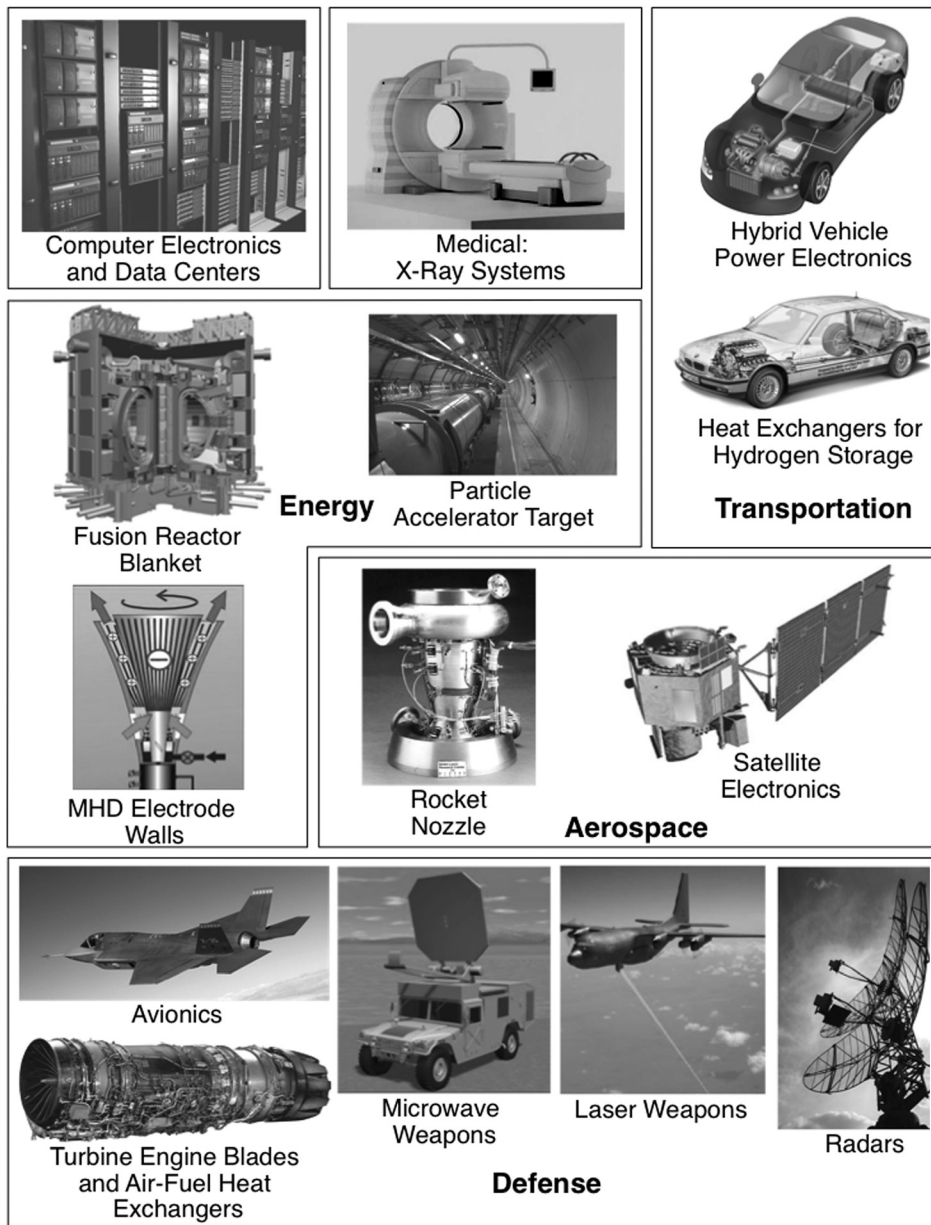
Fig. 1 Examples of computer, medical, transportation, energy, aerospace, and defense applications demanding high-heat-flux cooling schemes

Let us now consider a typical two-phase correlation for critical heat flux (CHF) in tubes. Clearly numerous, such correlations are available in the literature, but a typical correlation takes the form of [4]

$$\frac{q''_m}{G\,h_{fg}} = f\left(\frac{\rho_f}{\rho_g},\ \frac{G^2\,L}{\sigma\,\rho_f},\ \frac{c_{p,f}\,\Delta T_{\text{sub}}}{h_{fg}},\ \frac{L}{D},\ \frac{G}{\rho_f\,\sqrt{g\,D}},\ \dots\right)$$

$$= f\left(\Pi_1,\ \Pi_2,\ \Pi_3,\ \Pi_4,\ \Pi_5,\ \dots\right) \begin{cases} \Pi_{1,\min} < \Pi_1 < \Pi_{1,\max} \\ \Pi_{2,\min} < \Pi_2 < \Pi_{2,\max} \\ \Pi_{3,\min} < \Pi_3 < \Pi_{3,\max} \\ \Pi_{4,\min} < \Pi_4 < \Pi_{4,\max} \\ \Pi_{5,\min} < \Pi_5 < \Pi_{5,\max} \\ \quad\quad\quad . \\ \quad\quad\quad . \end{cases}$$

$$(2)$$

Notice here that, unlike the single-phase correlation in Eq. (1), the CHF correlation (a) consists of a dimensionless group that is a function of numerous other independent dimensionless groups, and (b) each of the independent groups is valid over a finite range. The development of a CHF correlation is hindered by the high cost of conducting two-phase experiments compared to their single-phase counterparts, which can have a strong bearing on the number of data points available from a given source. With such a limitation, the coverage of individual independent parameters is also very limited. This implies that a database that is consolidated from different experimental studies to construct a correlation of the form of Eq. (2) will be restricted to relatively narrow ranges of many independent parameters. In other words, the correlation is valid over a very small region of the multidimensional space encompassing all these independent parameters. This is the reason why thermal system designers are often confronted with the necessity to utilize correlations to design cooling systems with parameter ranges outside those for which the correlation is

intended. Such extrapolation of two-phase correlations is known to lead to highly inaccurate predictions.

The obvious alternative to empirical correlations is to develop theoretical models based on dominant underlying mechanisms. Examples include the Zuber et al. [5] model for pool boiling CHF from infinite horizontal surfaces, and the Galloway and Mudawar [6,7] model for flow boiling CHF. However, very few such theoretical models exist in the two-phase literature and, despite their theoretical formulation, these models require the use of one or more empirical constants to achieve closure and good predictions.

Objectives of Study. The primary objectives of this study are to discuss (a) the implementation of mini/microchannel, jet, and spray cooling configurations into practical cooling packages, (b) the advantages and drawbacks of each, (c) available predictive

tools, and (d) means to both enhance cooling performance and alleviate some of the disadvantages. It is important to emphasize that this paper is by no means a complete literature survey but rather a reflection of the author's own experiences and assessment.

2 Mini/Microchannel Cooling

Mini/microchannel cooling is commonly achieved with the aid of a heat sink that consists of a high conductivity substrate containing a large number of parallel, small diameter channels. The simplicity of heat sink design is a key reason behind its unprecedented popularity for cooling of electronics, lasers, avionics, and hybrid vehicle power electronics [2] and, more recently, air-fuel heat exchangers for high-Mach turbine engines [8] and hydrogen fuel cell storage systems [2,9]. Most microchannel heat sinks of
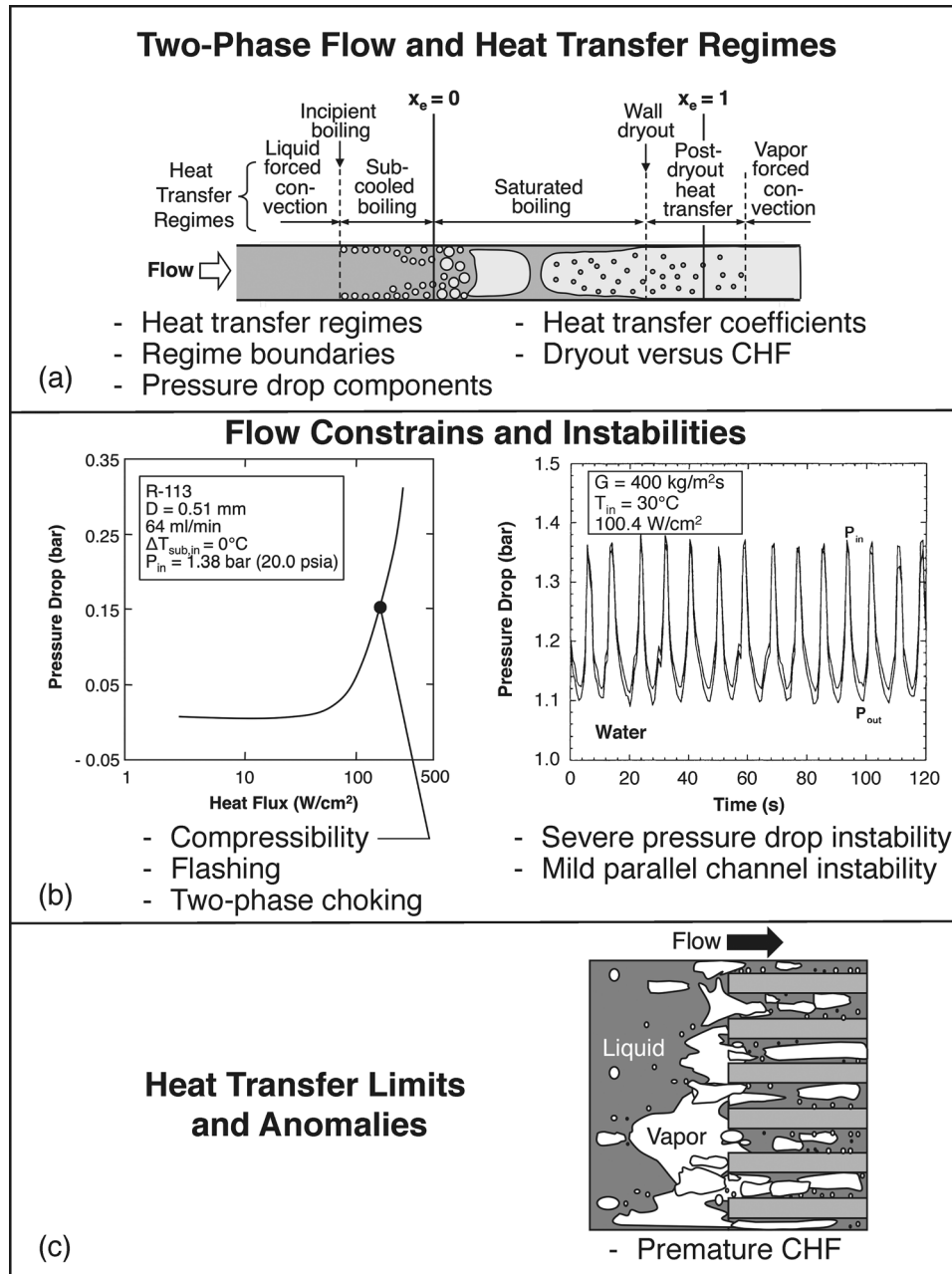

Fig. 2 Fundamental challenges to the understanding and prediction of fluid flow and heat transfer in mini/microchannel heat sinks: (*a*) difficulty ascertaining two-phase flow and heat transfer regimes, (*b*) two-phase flow constraints and instabilities, and (*c*) heat transfer limits and anomalies

practical interest possess diameters in the range of 0.1–0.6 mm, while diameters in minichannel heat sinks are typically in the range of 1.0–3.0 mm [2,10–12]. These heat sinks are therefore very compact and lightweight, and by allowing the coolant to undergo phase change along the channels, they provide heat transfer coefficients far greater than those of their single-phase counterparts by capitalizing upon the coolant's latent heat content rather than sensible heat alone. This greatly reduces the coolant flow rate required to dissipate the same amount of heat compared to a single-phase heat sink, which also helps reduce coolant inventory for the entire cooling system. Two-phase heat sinks also provide better temperature uniformity by maintaining surface temperatures close to the coolant's saturation temperature. However, two-phase microchannel heat sinks are not without shortcomings, and their implementation is hindered by the relatively limited understanding of two-phase transport behavior in small channel.

Figure 2 provides a summary of some of the challenges in both understanding and predicting two-phase flow and heat transfer in mini/microchannels. First and foremost, applying models or correlations that accurately capture the two-phase behavior prevalent inside the channel requires the determination of two-phase flow and heat transfer regimes, as well as the boundaries between regimes occurring concurrently along the channel. As shown in Fig. 2(a), with a subcooled inlet, liquid flow persists for a finite length until boiling commences on the channel wall, marking a transition to subcooled boiling. The saturated boiling region, which consists of bubbly, slug, and annular flow commences at the axial location where $x_e = 0$. The annular flow region is terminated at the point of wall dryout, downstream from which droplets are entrained in the vapor, and heat transfer is dominated by mist cooling. Eventually all droplets evaporate and the flow is converted to pure vapor. It is important to emphasize that not all of these regimes will occur along the channel. For example, a combination of high mass velocity and highly subcooled inlet results in predominantly subcooled nucleate boiling throughout the heat sink. On the other hand, a low mass velocity combined with a near-saturated inlet result in mostly annular flow. Clearly the prevailing flow regime has a profound influence on pressure drop, heat transfer coefficient, and CHF.

Figure 2(b) shows other challenges to predicting fluid flow and heat transfer in small channels, which stem from flow constraints and the potential for flow instabilities. In a study of flow boiling of R-113 in mini/microchannel heat sinks, Bowers and Mudawar [10–12] showed that, with a microchannel diameter of 0.51 mm, pressure drop escalates very rapidly following the initiation of boiling. This increase was attributed to flow acceleration caused by the axial reduction in two-phase mixture density. Associated with this high pressure drop are significant variations in the properties of the vapor and liquid, which can produce appreciable compressibility (specific volume variations of vapor and liquid with pressure) and/or flashing (vapor and liquid enthalpy variations with pressure), as well as increased likelihood of two-phase choking.

Figure 2(b) also shows pressure oscillations associated with instabilities commonly encountered in mini/microchannel heat sinks. While instabilities are commonplace in many types of two-phase systems [13,14], they can be especially problematic for mini/microchannel heat sinks. These instabilities take form of either severe pressure drop oscillation or mild parallel channel instability [15]. The severe pressure drop oscillation, which is the more serious of the two instabilities, is the result of communication of vapor generation in the channels with the compressible volume in the flow delivery system upstream of the heat sink. This instability can be eliminated by throttling, especially upstream of the heat sink. The mild parallel channel instability is the result of density wave oscillations within individual channels as well as feedback interaction between channels, and has a minor influence on cooling performance.

CHF is the most important cooling limit for any heat-flux-controlled boiling system. However, mini/microchannel heat sinks pose a unique challenge to determining this limit because of the

likelihood of premature CHF occurrence. This phenomenon is closely associated with two-phase flow instabilities and is encountered mostly at low mass velocities, where a larger volume of vapor is produced inside the channels. Illustrated in Fig. 2(c), it is triggered when the momentum of incoming liquid from the heat sink's upstream plenum is momentarily too weak to overcome the pressure drop across the channel. This causes vapor from the microchannels to flow backwards into the inlet plenum [16]. Two effective means to overcoming premature CHF are to (a) increase mass velocity, which helps prevent vapor backflow, and (b) increase inlet subcooling, which reduces vapor accumulation in the upstream plenum by condensation.

The compressibility and flashing effects and likelihood of two-phase choking are all reasons behind the need for accurate predictive tools for pressure drop in two-phase mini/microchannel heat sinks. The total pressure drop across the heat sink is the sum of several components that are associated with inlet contraction, upstream developing single-phase liquid region, subcooled two-
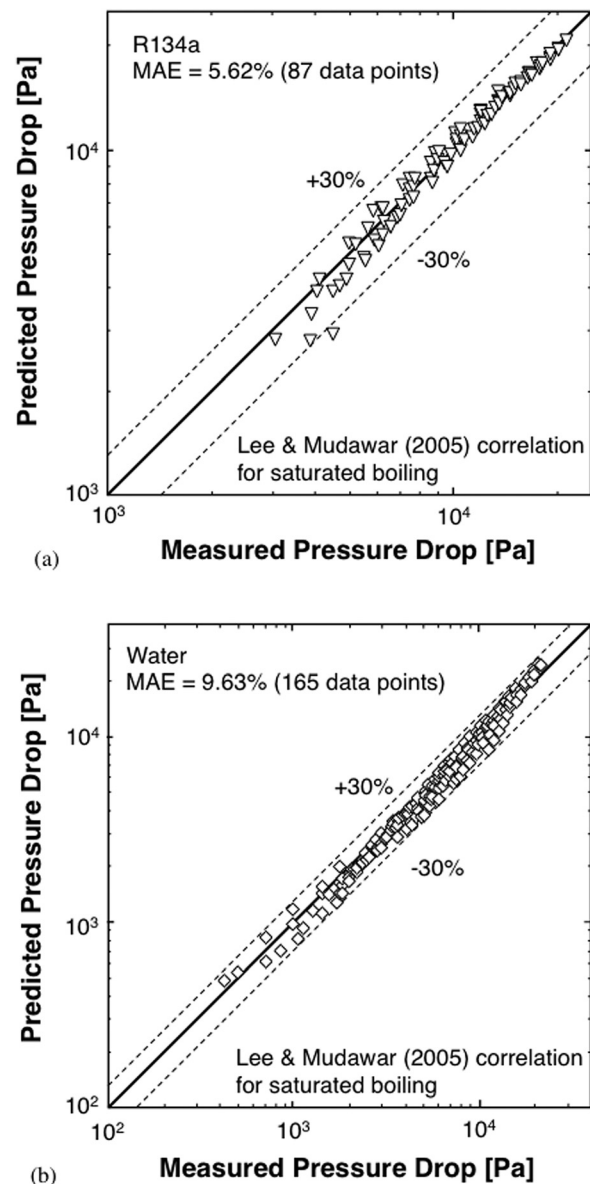

(a)

(b)

Fig. 3 Comparison of predictions of Lee and Mudawar correlation [18] for saturated boiling pressure drop in mini/microchannel heat sinks with (a) Lee and Mudawar R134a data [18] and (b) Qu and Mudawar water data [15]

Table 1   Relations for determination of two-phase pressure drop in mini/microchannel heat sinks

Total pressure drop: $\Delta P_{\text{tot}} = \Delta P_c + \Delta P_{1\phi,u} + \left(\Delta P_{2\phi,\text{sub}} + \Delta P_{2\phi,\text{sat}}\right) + \Delta P_{1\phi,d} + \Delta P_e$

1. Inlet contraction [22]:

$$\Delta P_c = \frac{G^2 v_f}{2}\left[\left(\frac{1}{C_c}-1\right)^2 + \left(1-\sigma_c^2\right)\right]\left[1 + \frac{v_{fg}x_{e,\text{in}}}{v_f}\right]$$

where $\quad \sigma_c = \dfrac{W_{\text{ch}}H_{\text{ch}}N}{W_p H_p}\quad$ and $\quad C_c = \begin{cases} 1 - \dfrac{1-\sigma_c}{2.08(1-\sigma_c)+0.5371} & \text{for liquid inlet} \\ 1.0 & \text{for two-phase inlet} \end{cases}$

2. Upstream single-phase liquid region [19]:

$$\Delta P_{1\phi,u} = \frac{2f_{1\phi,u}G^2 L_{1\phi,u}v_f}{D_h}$$

3. Subcooled liquid region [22]:

$$\frac{\Delta P_{2\phi,\text{sub}}}{\Delta P_{1\phi}} = 20.73\left(\frac{c_{p,f}\Delta T_{\text{sub,in}}}{h_{fg}}\right)^{-0.98}\left(\frac{W_{\text{ch}}}{H_{\text{ch}}}\right)^{0.42}\left(\frac{L}{D_h}\right)^{-0.54}\frac{L_{2\phi,\text{sub}}}{L_{2\phi,\text{sat}}}$$

4. Saturated liquid region: $\Delta P_{2\phi,\text{sat}} = \Delta P_{2\phi,\text{sat},F} + \Delta P_{2\phi,\text{sat},A}$

    4.1 Frictional component [18]:

$$\Delta P_{2\phi,\text{sat},F} = \frac{2G^2 L_{2\phi,\text{sat}}}{D_h x_{e,\text{out}}}\int_0^{x_{e,\text{out}}} f_f(1-x_e)^2 v_f \phi_f^2 \, dx_e$$

Two-phase multiplier: $\phi_f^2 = 1 + \dfrac{C}{X} + \dfrac{1}{X^2}$

Lockhart–Martinelli parameter: $X^2 = \dfrac{(dP/dz)_f}{(dP/dz)_g}$

Empirical constant in two-phase multiplier:

      Laminar liquid-laminar vapor: $\quad C = 2.16\text{Re}_{fo}^{0.047}\text{We}_{fo}^{0.60}$

      Laminar liquid-turbulent vapor: $\quad C = 1.45\text{Re}_{fo}^{0.25}\text{We}_{fo}^{0.23}$

      Turbulent liquid-turbulent vapor: $\quad C = 0.048\text{Re}_{fo}^{0.451}$

where $\quad -\left(\dfrac{dP}{dz}\right)_f = \dfrac{2f_f v_f G^2(1-x_e)^2}{D_h}, \; -\left(\dfrac{dP}{dz}\right)_g = \dfrac{2f_g v_g G^2 x_e^2}{D_h}, \text{Re}_{fo} = \dfrac{GD_h}{\mu_f}, \quad$ and $\quad \text{We}_{fo} = \dfrac{G^2 D_h}{\sigma \rho_f}$

    4.2 Accelerational pressure drop [18]:

$$\Delta P_{2\phi,\text{sat},A} = G^2\left\{\left[\frac{v_g x_{e,\text{out}}^2}{\alpha_{\text{out}}} + \frac{v_f\left(1-x_{e,\text{out}}\right)^2}{(1-\alpha_{\text{out}})}\right] - \left[\frac{v_g x_{e,\text{in}}^2}{\alpha_{\text{in}}} + \frac{v_f\left(1-x_{e,\text{in}}\right)^2}{(1-\alpha_{\text{in}})}\right]\right\}$$

where $\quad \alpha = \left[1 + \left(\dfrac{1-x_e}{x_e}\right)\left(\dfrac{v_f}{v_g}\right)^{2/3}\right]^{-1}$

5. Downstream vapor region [19]:

$$\Delta P_{1\phi,d} = \frac{2f_{1\phi,d}G^2 L_{1\phi,d}v_f}{D_h}$$

6. Downstream pressure recovery [22]:

$$\Delta P_e = G^2 \sigma_e(\sigma_e - 1)v_f\left[1 + \frac{v_{fg}x_{e,\text{out}}}{v_f}\right]$$

where $\quad \sigma_e = \dfrac{W_{\text{ch}}H_{\text{ch}}N}{W_p H_p}$

phase region (for subcooled inlet conditions), saturated two-phase region, downstream vapor region, and outlet pressure recovery.

Most studies on pressure drop in two-phase mini/microchannel heat sinks are centered on the saturated two-phase region that contributes the largest percentage of total pressure drop. Three different approaches have been used for this purpose: (1) homogeneous equilibrium model (HEM), used in conjunction with an appropriate two-phase friction factor or two-phase viscosity model [10], (2) semiempirical models, based mostly on the Lockhart–Martinelli separated flow model (SFM) [17], and (3) theoretical models [15]. Lockhart–Martinelli-type formulations have been especially popular in recent years because of their

effectiveness in predicting pressure drop data for different coolants as shown in Fig. 3.[1]

Despite the overwhelming contribution of the two-phase region, a complete pressure drop model must be based on accurate models for all component of pressure drop, as well as be able to accurately predict the axial extent of individual flow and heat transfer regimes. The extent of the upstream developing and fully developed portions of the single-phase liquid region can be determined from a relation such that of Shah and London [19],

---

[1]References cited in Fig. 3 are [15,18].

Table 2 Relations for determination of heat transfer coefficient in mini/microchannel heat sinks

1. Upstream thermal developing liquid region [22]:

$$\frac{h_{1\phi,f}D_h}{k_f} = \mathrm{Nu}_{1\phi,f} = \begin{cases} \left\{\left[1.54\left(\dfrac{L_{1\phi,f}}{\mathrm{Re}_{fo}\mathrm{Pr}_f D_h}\right)^{-0.33}\right]^4 + \mathrm{Nu}_3^4\right\}^{1/4} & \text{developing laminar} \\[12pt] 0.023\mathrm{Re}_{fo}^{0.8}\mathrm{Pr}_f^4\left[1 + \dfrac{(L_{1\phi,f}/D_h)^{-0.9}}{10\mathrm{Pr}_f^{1/6}}\left(0.68 + \dfrac{3000}{\mathrm{Re}_{fo}^{0.81}}\right)\right] & \text{developing turbulent} \end{cases}$$

where $\quad \mathrm{Nu}_3 = 8.235\left(1 - 1.833\beta + 3.767\beta^2 - 5.814\beta^3 + 5.361\beta^4 - 2.0\beta^5\right),$

$$\beta = W_{\mathrm{ch}}/H_{\mathrm{ch}}, \mathrm{Re}_{fo} = \frac{GD_h}{\mu_f}$$

2. Subcooled two-phase region [24]:

$$h_{2\phi,\mathrm{sub}} = 90.0\left(\frac{q''}{Gh_{fg}}\right)^{0.9}\left(\frac{c_{p,f}\Delta T_{\mathrm{sub,in}}}{h_{fg}}\right)^{-0.98}\mathrm{We}^{*0.15}\beta^{0.42}h_{1\phi,f}^*$$

where $\quad \mathrm{We}^* = \dfrac{G^2 D_h}{\left(\rho_f - \rho_g\right)\sigma}, \dfrac{h_{1\phi,f}^* D_h}{k_f} = \begin{cases} \mathrm{Nu}_3 & \text{laminar} \\ 0.023\mathrm{Re}_f^{0.8}\mathrm{Pr}_f^{0.4}k_f/D_h & \text{turbulent} \end{cases}$

3. Saturated two-phase region [24]:

$$h_{\mathrm{sat}} = \begin{cases} 3.856 X^{0.267} h_{1\phi,f} & \text{for } 0 \le x_e < 0.05 \\[8pt] 436.48\left(\dfrac{q''}{Gh_{fg}}\right)^{0.522}\mathrm{We}_{fo}^{0.351} X^{0.665} h_{1\phi,f} & \text{for } 0.05 \le x_e < 0.55 \\[8pt] \mathrm{Max}\left\{\left(108.6 X^{1.665} h_{1\phi,g}\right), h_{1\phi,g}\right\} & \text{for } 0.55 \le x_e \le 1.0 \end{cases}$$

where $\quad \mathrm{We}_{fo} = \dfrac{G^2 D_h}{\sigma \rho_f}$

4. Downstream single-phase vapor region [19]:

$$\frac{h_{1\phi,g}D_h}{k_g} = \mathrm{Nu}_{1\phi,g} = \begin{cases} \mathrm{Nu}_3 & \text{laminar} \\ 0.023\,\mathrm{Re}_g^{0.8}\mathrm{Pr}_g^{0.4}k_g/D_h & \text{turbulent} \end{cases}$$

where $\quad \mathrm{Re}_g = \dfrac{Gx_e D_h}{\mu_g}$

$$L_{1\phi,u,\mathrm{dev}} = \left(0.06 + 0.07\beta - 0.04\beta^2\right)\left(\frac{GD_h}{\mu_f}\right)D_h \qquad (3)$$

Another important transition point along the channel is location of the onset of boiling. This point can be determined either by using a theoretical model for incipient boiling in mini/microchannels [20] or Sato and Matsumura's relation [21]

$$q''_{\mathrm{ch,ONB}} = \frac{k_f h_{fg} \rho_g (T_w - T_{\mathrm{sat}})^2}{8\sigma T_{\mathrm{sat}}} \qquad (4)$$

The above relation is used to determine the location where subcooled boiling is initiated. The subcooled boiling region extends over a length $L_{2\phi,\mathrm{sub}}$ from the location of boiling initiation to the location where $x_e = 0$. The saturated boiling extends over a length $L_{2\phi,\mathrm{sat}}$ between the locations where $x_e = 0$ and 1.

Table 1 provides a summary of pressure drop relations for the different regions of the channel. Relations for the upstream single-phase liquid friction factor $f_{1\phi,u}$ are provided by Kim and Mudawar [22]. Table 2 provides a corresponding summary for the heat transfer correlations. Figure 4 shows a comparison of predictions of the correlation recommended for the saturated two-phase region [24] with data for R134a and water.

For CHF, the following correlation was developed by Lee and Mudawar [23] by modifying the Hall and Mudawar [24] ultrahigh CHF formulation for water flow in small tubes,
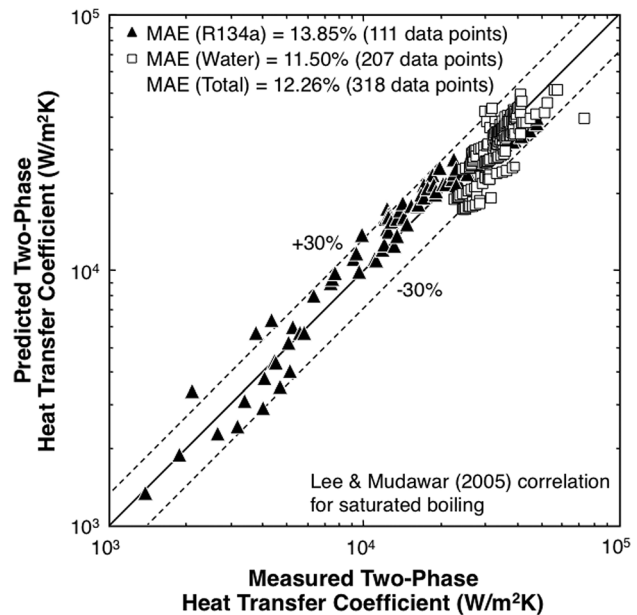

Fig. 4 Comparison of predictions of Lee and Mudawar [24] correlation for saturated boiling heat transfer coefficient in mini/microchannel heat sinks with Lee and Mudawar R134a data [24] and Qu and Mudawar water data [15]

$$q''_{m,h} = 0.0332 G h_{fg} \mathrm{We}_{D_{eq}}^{-0.114} \left(\frac{v_g}{v_f} \right)^{-0.681}$$

$$\times \left[1 + 0.684 \left(\frac{v_g}{v_f} \right)^{0.832} \frac{\Delta h_{sub,in}}{h_{fg}} \right]$$

$$\times \left[1 + 0.0908 \mathrm{We}_{D_{eq}}^{-0.235} \left(\frac{v_g}{v_f} \right)^{0.151} \frac{L}{D_{eq}} \right]^{-1} \quad (5)$$

where $q''_{m,h}$ is the average CHF along the heated walls of the microchannel, $D_{eq} = 4.364 \, D_h / \mathrm{Nu}_3$, and $\mathrm{We}_{D_{eq}} = \left(G^2 D_{eq} \right) / \left(\sigma \rho_f \right)$.

While most modern cooling applications favor the use of inert and dielectric coolants, Mudawar and Bowers [25] explored water cooling for ultra-high-flux applications such as fusion reactors. A combination of very high mass velocity ($G = 120{,}000 \, \mathrm{kg/m^2 \, s}$), small tube diameter ($D = 0.406 \, \mathrm{mm}$), and high subcooling yielded the highest CHF of $27{,}600 \, \mathrm{W/cm^2}$ ever reported in the literature for a uniformly heated tube. The CHF correlation of Hall and Mudawar [24] is recommended for these water cooling conditions.

3 Jet-Impingement Cooling

Liquid jet impingement is one of the most popular means for achieving very high heat transfer coefficients, especially when the coolant undergoes phase change [26–29]. Most jet-impingement cooling packages employ jets that are issued normal to the heat-dissipating surface through a circular or slot orifice. The heat transfer coefficient is highest in the impingement zone directly below the orifice and decreases away from the impingement zone. This decrease can lead to substantial nonuniformity in surface temperature. Multiple jets are therefore used, not only to enhance temperature uniformity, but to increase the average heat transfer coefficient as well [30]. Overall, jet-impingement cooling

demands higher coolant flow rates than mini/microchannel and spray cooling, but its pressure drop is comparatively modest.

The heat transfer literature includes a substantial number of articles addressing both the fundaments and practical implementation of jet-impingement cooling. But the vast majority of these articles concern single-phase cooling, and the knowledge base for two-phase cooling is quite sparse. Figure 5 shows a summary of key fundamental issues governing two-phase jet-impingement cooling. The first is jet formation at the nozzle itself, including the influence of shape, size, and geometry of the nozzle. As the jet emerges from the nozzle, it thickens due to due to resistance from, and entrainment of, surrounding liquid as shown in Fig. 5(a). Jet thickening influences both the size of the impingement zone and spatial variation of the heat transfer coefficient along the impingement surface. A wall jet is formed along the impingement surface downstream from the impingement zone. Like the flow exiting the nozzle, the wall jet is influenced by resistance from, and entrainment of, surrounding liquid. The wall jet flow generally starts laminar but can turn turbulent depending on operating conditions. But the wall jet flow and heat transfer coefficient are dictated mostly by bubble growth and departure. As shown in Fig. 5(b) for a free jet, an axial increase in the void fraction causes the wall jet to thicken substantially, which, along with the detrimental momentum of vapor normal to the surface, triggers vigorous splashing of the wall jet liquid away from the surface, which can be a precursor to CHF [26,29,31,32]. A popular tactic to overcoming this splashing phenomenon is to confine the flow between the nozzle and the impingement surface [30,33–35]. With a confined jet, the wall jet may quickly develop into two-phase channel flow. A clear
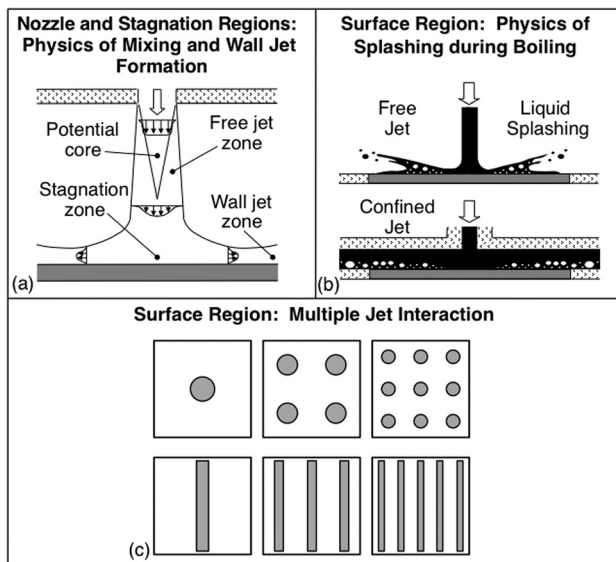
Fig. 5 Fundamental physics of jet-impingement cooling: (a) Influence of orifice size and shape on flow characteristics, effect of orifice-to-wall distance on size of stagnation zone, transition from laminar to turbulent flow, and boiling incipience downstream from the stagnation zone. (b) Splashing of wall jet liquid for free jet, splash prevention to increase CHF for confined jet, and wall jet versus two-phase channel flow behavior for confined jet. (c) Heat transfer and CHF enhancement with multiple jets, interaction between wall jets and instabilities in the flow of spent fluid for multiple jets, and manufacturing tolerance concerns for multiple small jets.
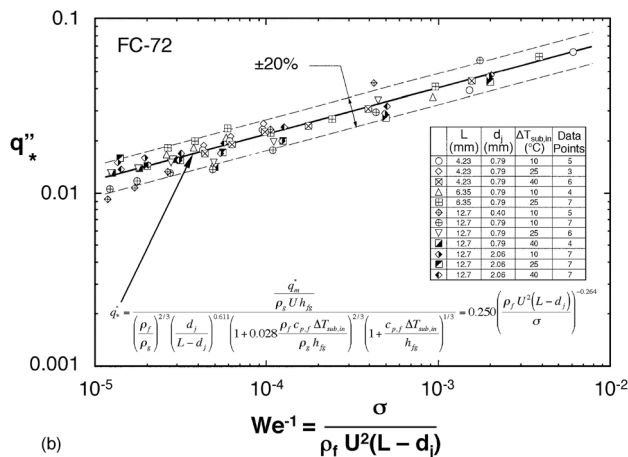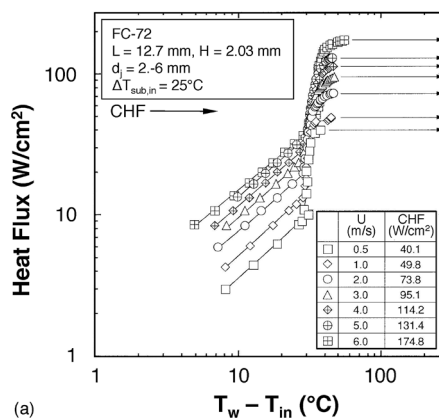
Fig. 6 (a) Variations of single-phase cooling and nucleate boiling for circular FC-72 jets with jet velocity. (b) Correlation of CHF data for circular FC-72 jets for different jet velocities, jet diameters, surface widths, and subcoolings (Johns and Mudawar [36]).

understanding of this confined flow configuration is of vital importance to the design of the cooling module. By far, the most difficult task in designing a practical two-phase jet-impingement cooling system utilizing multiple circular or slot jets (Fig. 5(c)) is the complexity of fluid interactions between jet impingement zones and likelihood of instabilities in the flow of spent fluid.

Johns and Mudawar [34] examined the influence of jet diameter, jet velocity, surface width, and subcooling on jet-impingement cooling of FC-72 for single circular nozzle configurations. Figure 6(a) shows the influence of jet velocity on the boiling curve. Increasing jet velocity is shown increasing the heat transfer coefficient in the single-phase region. There is a noticeable convergence of data in the nucleate boiling region regardless of flow velocity. But the velocity influence is very noticeable again in the upper region of nucleate boiling, which is manifest by a monotonic increase in CHF with increasing jet velocity. Despite

this and many other published databases for two-phase jet impingement, to the author's best knowledge, no reliable correlation has been recommended for the nucleate boiling regime. Figure 6(b) shows CHF data from the Johns and Mudawar study successfully correlated by the relation

$$\frac{q_m''}{\rho_g \, U \, h_{fg}} = 0.250 \left(\frac{\rho_f \, U^2 \, (L - d_j)}{\sigma} \right)^{-0.264} \left(\frac{\rho_f}{\rho_g} \right)^{2/3} \left(\frac{d_j}{L - d_j} \right)^{0.611}$$

$$\times \left(1 + 0.028 \, \frac{\rho_f \, c_{p,f} \, \Delta T_{\mathrm{sub,in}}}{\rho_g \, h_{fg}} \right)^{2/3} \left(1 + \frac{c_{p,f} \, \Delta T_{\mathrm{sub,in}}}{h_{fg}} \right)^{1/3}$$

$$(6)$$

where U, L, and d_j are mean jet velocity, width of impingement surface, and jet diameter, respectively.
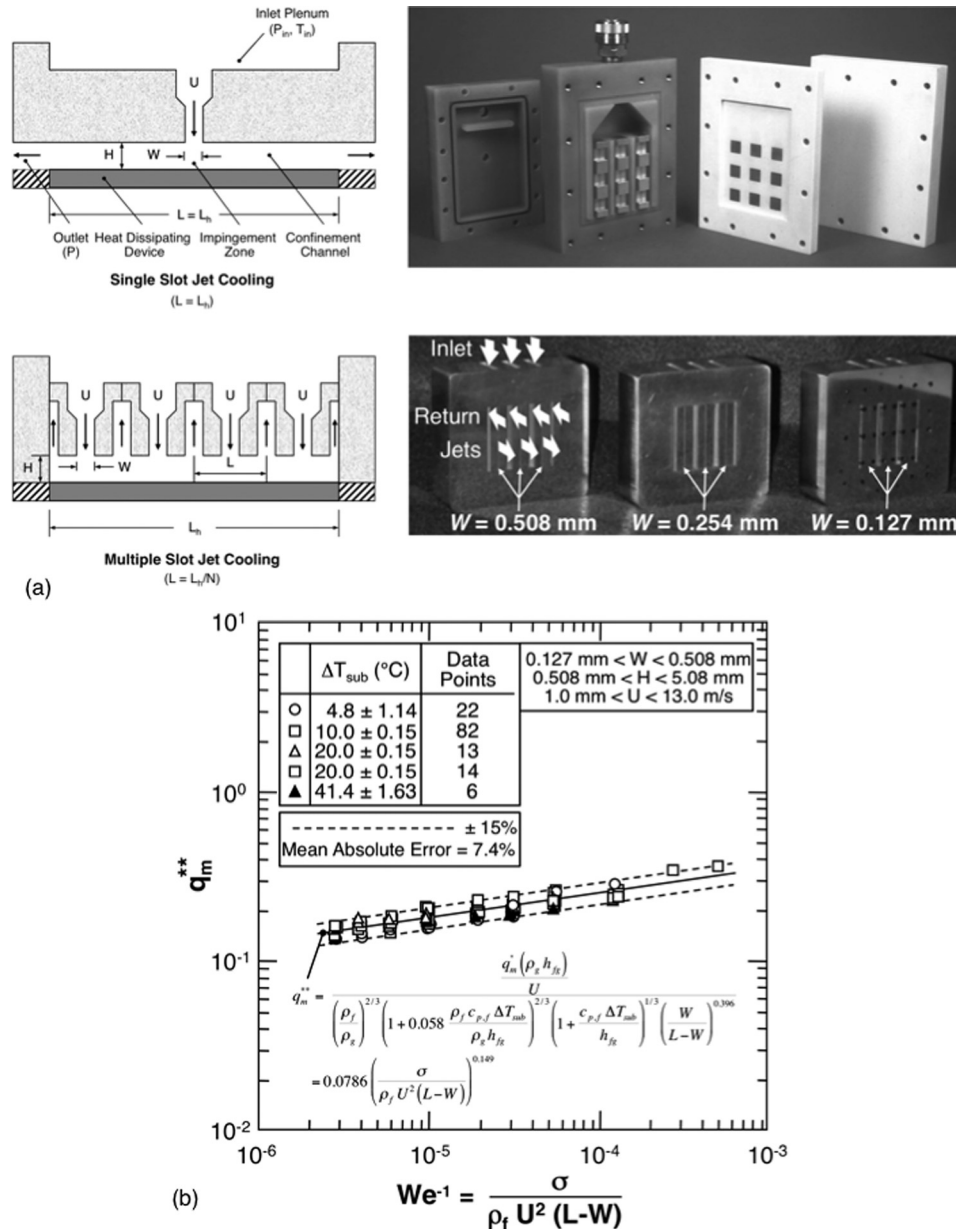

(a)

(b)

Fig. 7 (*a*) **Confined slot-jet impingement cooling modules using single jets (Mudawar and Wadsworth [35]) and multiple jets (Meyer et al. [37]). (*b*) Correlation of CHF data for single FC-72 slot jets for different jet velocities, jet widths, nozzle-to-surface distances, and subcoolings (Mudawar and Wadsworth [35]).**

Figure 7(a) shows different examples of two-phase jet-impingement cooling with confined slot jets using single jets [33] and multiple jets [35]. Using single confined slots jets, Mudawar and Wadsworth [33] developed a cooling module for a 3×3 array of heat sources, which was capable of uniformly supplying coolant to, and rejecting it from, each heat source. Using FC-72 as coolant, over 300% increase in CHF was achieved when the jet velocity was increased from 1 to 11 m/s. Significant CHF enhancement was also achieved by increasing the coolant's subcooling. An important practical conclusion from their study is that jet velocity has a stronger influence on CHF than jet width. This means flow rate requirements can be reduced simply by choosing a smaller jet width. Figure 7(b) shows Mudawar and Wadsworth data for different jet widths, nozzle-to-surface distances, jet velocities, and subcoolings correlated with a mean absolute error of 7.4% according to the relation

$$\frac{q''_m}{\rho_g\, U\, h_{fg}} = 0.0786 \left(\frac{\rho_f\, U^2\, (L-W)}{\sigma}\right)^{0.149} \left(\frac{\rho_f}{\rho_g}\right)^{2/3} \left(\frac{W}{L-W}\right)^{0.396}$$

$$\times \left(1 + 0.058\, \frac{\rho_f\, c_{p,f}\, \Delta T_{\text{sub,in}}}{\rho_g\, h_{fg}}\right)^{2/3} \left(1 + \frac{c_{p,f}\, \Delta T_{\text{sub,in}}}{h_{fg}}\right)^{1/3} \tag{7}$$

where W and H are the jet width and nozzle-to-surface distance, respectively. Confined two-phase slot-jet cooling also shows great potential when implemented in conjunction with surface enhancement. Figure 8 shows CHF for this configuration is enhanced by over 214% and 178% with microgroove and microstud enhanced surfaces, respectively [36].

4 Spray Cooling

Designing a spray cooling system is by no means a straightforward endeavor. Cooling system designers are quickly confronted with the task of configuring a system whose performance depends on an usually large number of parameters. Aside from nozzle type and coolant, cooling performance is influenced by droplet size, droplet velocity, volumetric flux, and the spatial distributions of these three parameters; in addition to spray angle, nozzle orientation angle, and orifice-to-surface distance [37]. Clearly the design of a spray cooling system requires a comprehensive, systematic methodology that tackles the influences of all these parameters with a high degree of accuracy, and which is applicable to coolants with drastically different thermophysical properties.

Early research on spray cooling centered mostly on high-temperature cooling in metal processing operations. Emphasis shifted during the last three decades to the implementation of spray cooling in relatively low temperature applications, such as those depicted in Fig. 1. Unfortunately, the spray cooling literature for low temperature applications is quite sparse. Most published studies point to volumetric flux Q'' as the dominant spray parameter influencing cooling [38,39]. This parameter is defined as the flow rate impacting an infinitesimal portion of the surface divided by the area of the same portion. Mudawar and Valentine [37] measured and correlated spray cooling data for all regimes of the boiling curve (single-phase cooling and nucleate, transition, and film boiling) for water sprays. Estes and Mudawar [32] developed an empirical CHF relationship for FC-72, FC-87, and water sprays based on local volumetric flux, Q'', and Sauter mean diameter (SMD) d_{32}. Other noteworthy literature includes studies on nucleate boiling by Ghodbane and Holman [40], Holman and Kendall [41], and Rini et al. [42], and on CHF by Cho and Wu [43], Chen et al. [44], and Lin and Ponnappan [45].

Spray cooling provides several important benefits, such as high heat transfer coefficients, high CHF, and superior surface temperature uniformity for a relatively large surface. Cooling effectiveness is realized by breaking the liquid into a dispersion of fine
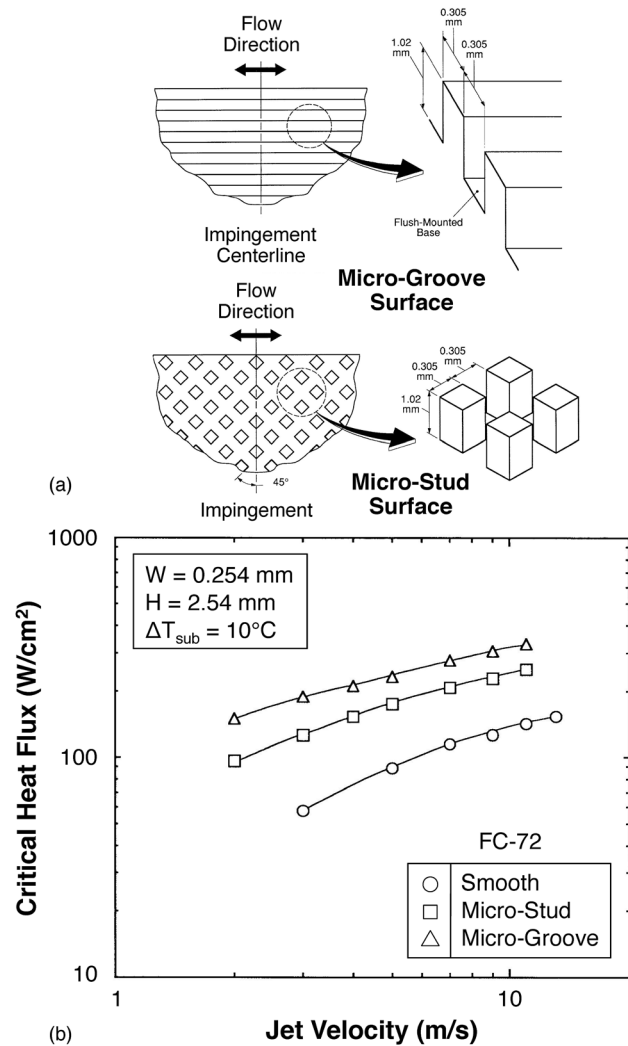

Fig. 8 (*a*) Microgroove and microstud surfaces used to enhance single confined slot-jet impingement cooling. (*b*) Variation of CHF with jet velocity for smooth and enhanced surfaces (Wadsworth and Mudawar [38]).

droplets having large surface-area-to-volume ratio, which acquire multiple trajectories and impact a broad surface area. Despite these benefits, implementation of spray cooling has been hindered by relatively poor understanding of the influence of the spray parameters on cooling performance, and the lack of long-term repeatability of performance because of both corrosion and erosion of the intricate flow passages of the spray nozzle [46].

Figure 9 provides a summary of fundamental mechanisms that govern spray cooling. Effective droplet breakup is key to achieving large surface-area-to-volume ratio in the form fine droplets. As shown in Fig. 9(a), the breakup commences with formation of unstable liquid sheets, which break up further first into ligaments and eventually fine droplets. A sufficiently large orifice-to-surface distance is therefore required to achieve fully developed liquid breakup. Another fundamental issue is the spatial distributions of key droplet parameters, such as Sauter mean droplet diameter d_{32}, mean droplet velocity U_m, and especially volumetric flux Q'' (Fig. 9(b)). The spatial variations of these parameters are complicated by interaction between adjacent sprays (Fig. 9(b)) which is often used to promote surface temperature uniformity. Cooling effectiveness is also a function of droplet impact with the surface (Fig. 9(c)) which is further complicated by liquid buildup on the surface.
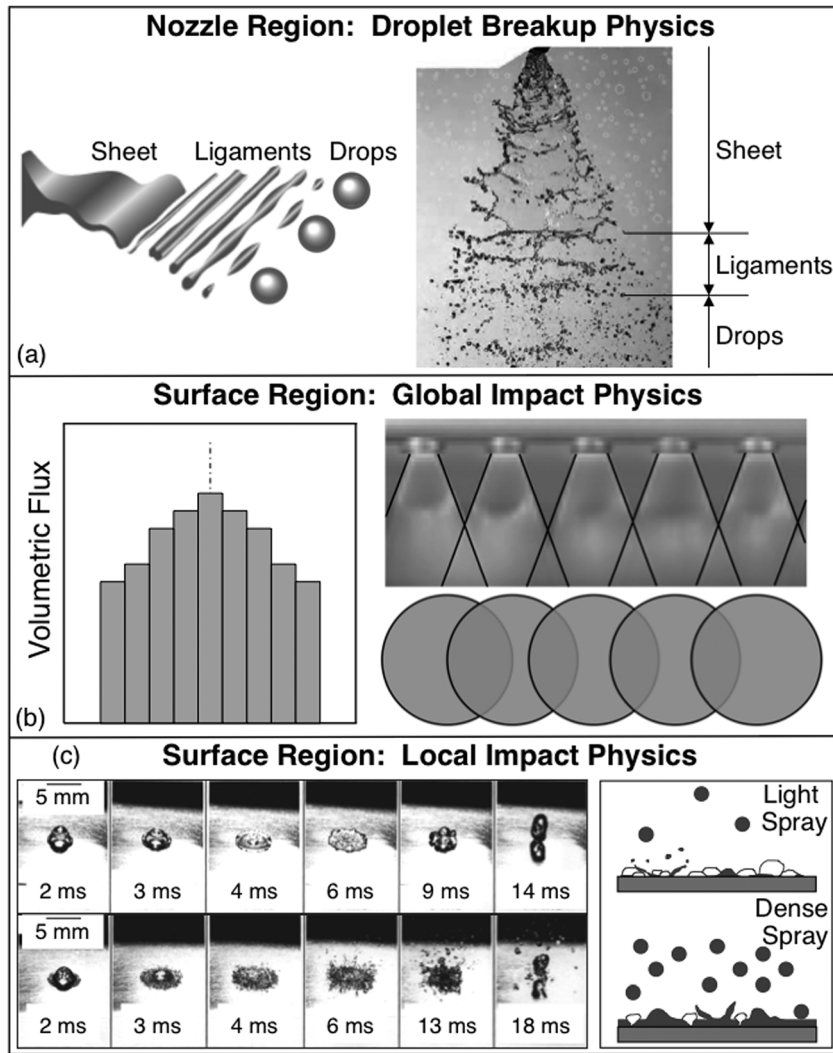
Fig. 9 Fundamental physics of spray cooling: (*a*) Droplet breakdown, distance from orifice required to ensure fully developed breakup, and influence of nozzle type, orifice size, and pressure drop on mass flow rate and mean droplet size and velocity. (*b*) Volumetric flux distribution on impact surface and required overlap between impact areas to ensure uniform surface temperature. (*c*) Impact dynamics and heat transfer of individual droplets, liquid film buildup (dense versus light sprays), nucleate boiling heat transfer, and critical heat flux (CHF).

Presented below is a summary of available predictive models and correlations for spray cooling, as well as recommendations for future research. The methodology presented here concerns pressure spray nozzles that are preferred for electronic cooling applications.

For full-cone spray nozzles, d_{32} is determined from the nozzle pressure drop ΔP and orifice diameter d_o based on the nozzle flow Weber and Reynolds numbers according to the following relation by Estes and Mudawar [47]:

$$\frac{d_{32}}{d_o} = 3.67 \left[\text{We}_{d_0}^{1/2} \text{Re}_{d_o} \right]^{-0.259} \quad (8)$$

where

$$\text{We}_{d_o} = \frac{\rho_g \left(2 \Delta P / \rho_f \right) d_0}{\sigma} \quad (9)$$

and

$$\text{Re}_{d_o} = \frac{\rho_f \left(2 \Delta P / \rho_f \right)^{1/2} d_0}{\mu_f} \quad (10)$$

As shown in Fig. 10, the spatial distribution of volumetric flux for a spray impacting a flat surface located a distance H from the orifice can be described with the aid of a point source model which assumes that the volumetric flux is uniform along any spherical surface centered at the orifice [48]. The uniform flux for a spherical surface of radius H yields a volumetric flux on the impact surface that decreases radially from the spray centerline. This model yields the following distribution for local volumetric flux Q'' along the surface as a function of H, radial distance r, and the spray's cone angle θ:

$$\frac{Q''}{\overline{Q}''} = \frac{1}{2} \left[\frac{\tan^2(\theta/2)}{1 - \cos(\theta/2)} \right] \frac{1}{\left[1 + \left(\frac{r}{H} \right)^2 \right]^{3/2}} \quad (11)$$

Rybicki and Mudawar [49] derived the following correlation for the nucleate boiling region for spray cooling based on data for different fluids and normal upward-facing and normal downward-facing sprays:
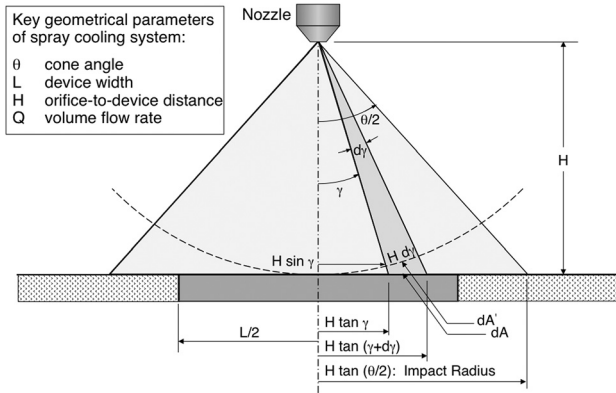
**Fig. 10 Spray volumetric flux distribution based on uniform point source model (Mudawar and Estes [50])**

$$\frac{q'' \, d_{32}}{\mu_f h_{fg}} = 4.79 \times 10^{-3} \left(\frac{\rho_f}{\rho_g} \right)^{2.5} \left(\frac{\rho_f \bar{Q}^2 d_{32}}{\sigma} \right)^{0.35} \left(\frac{c_{p,f} \left(T_s - T_f \right)}{h_{fg}} \right)^{5.75} \tag{12}$$

As shown in Fig. 11(a), the same correlation was later validated by Visaria and Mudawar [50] for accuracy against inclined spray data.

Estes and Mudawar [47,48] demonstrated experimentally that CHF for a normal full-cone spray is initiated at locations of weakest volumetric flux along the surface. Visaria and Mudawar [50] extended this correlation by accounting for the influence of spray orientation relative to the surface. As shown in Fig. 11(b), this correlation provides good predictions for different fluids and normal upward-facing, normal downward-facing, and inclined sprays. The CHF correlation,
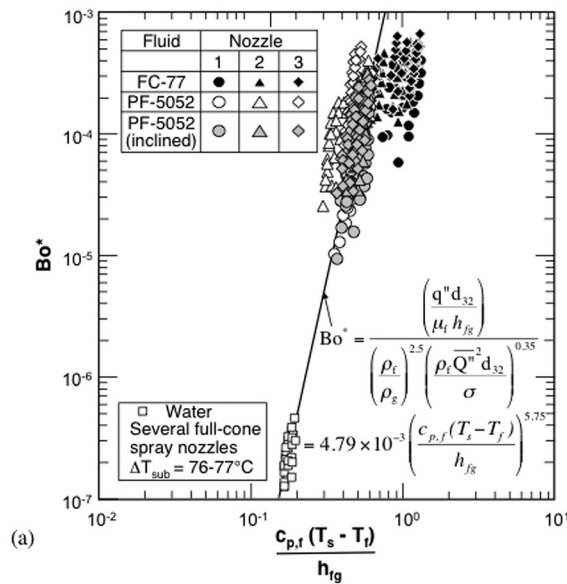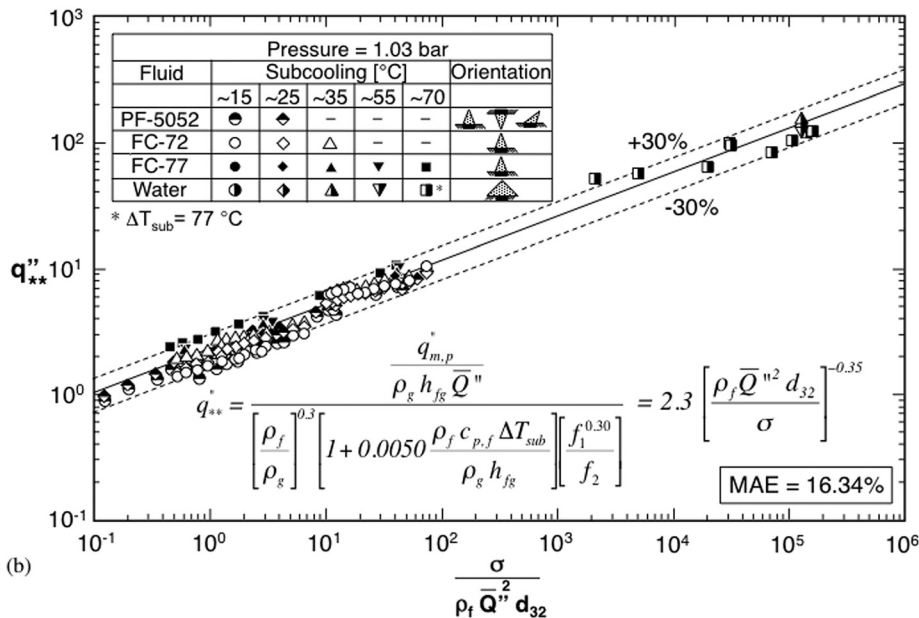
Fig. 11 Correlations for (a) nucleate boiling and (b) CHF for upward-facing, downward-facing, and inclined PF-5052 sprays, downward-facing FC-77 sprays, and downward-facing water sprays (Visaria and Mudawar [52])
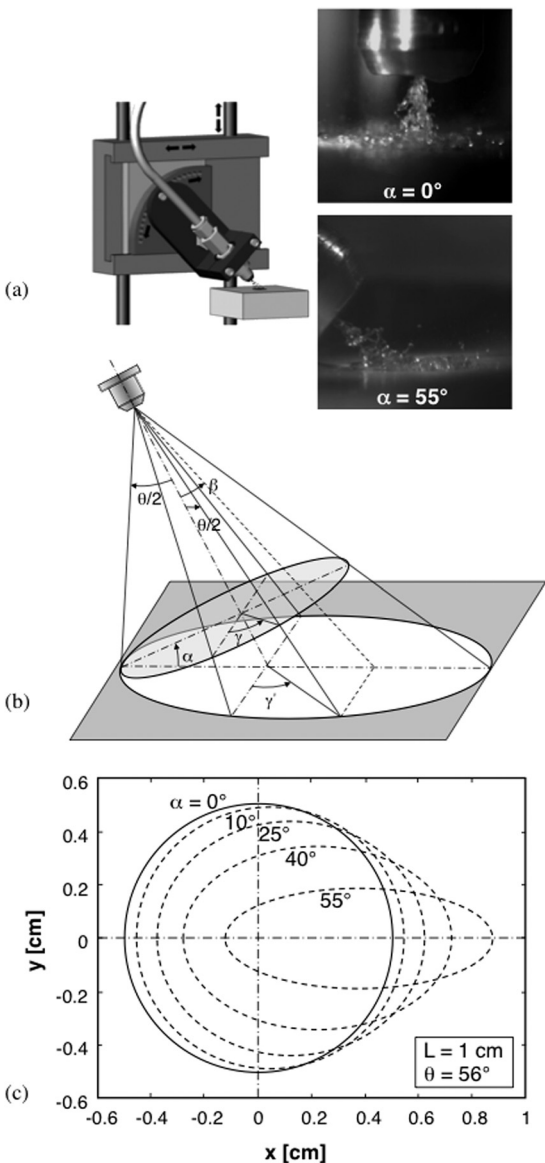
Fig. 12 (*a*) Images of normal and inclined sprays. (*b*) Model of inclined spray impacting a square surface. (*c*) Variation of spray impact area with inclination angle (Visaria and Mudawar [52]).

$$\frac{q''_m}{\rho_g h_{fg} \overline{Q}''} = 2.3 \left(\frac{\rho_f}{\rho_g}\right)^{0.3} \left(\frac{\rho_f \bar{Q}''^2 d_{32}}{\sigma}\right)^{-0.35}$$

$$\times \left(1 + 0.0050 \frac{\rho_f \, c_{p,f} \Delta T_{sub}}{\rho_g \, h_{fg}}\right) \left(\frac{f_1^{0.30}}{f_2}\right) \quad (13)$$

includes a multiplier $\left(f_1^{0.30}/f_2\right)$ that accounts for the influence of spray orientation on CHF; $\left(f_1^{0.30}/f_2\right) = 1$ for normal sprays.

Several changes from the simple spray configuration depicted in Fig. 10 have been attempted in the implementation of spray cooling. The two most relevant are the use of spray orientations other than normal, and sprays with overlapping impact areas. Inclined sprays have been proposed for electronics cooling to reduce the height of the cooling package by reducing the orifice-to-surface distance as depicted in Fig. 12(*a*). Figure 12(*b*) shows a schematic of an inclined spray whose orifice-to-surface distance is adjusted such that the major axis of the impact area just inscribes a square surface in order to maximize CHF. Figure 12(*c*) shows the variation of spray impact area with orientation angle α. A
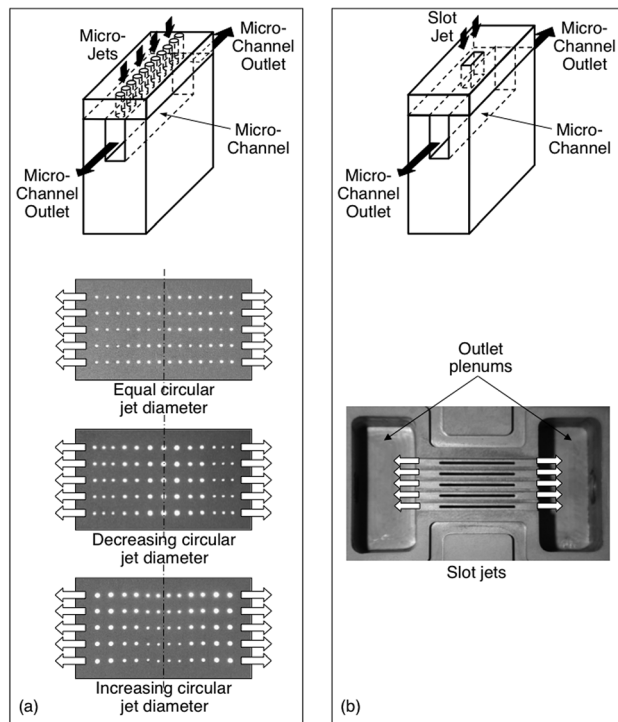
Fig. 13 Hybrid cooling scheme combining jet-impingement with mini/microchannel cooling using (*a*) circular jets and (*b*) slot jets (Sung and Mudawar [53,54])

detailed discussion of how the function $\left(f_1^{0.30}/f_2\right)$ in Eq. (13) is determined for different orientations is provided by Visaria and Mudawar [50]. The same reference also provides a technique for assessing the influence of overlap. In general, increasing volumetric flux for overlapping spray impact areas increases the nucleate boiling heat transfer coefficient but not CHF.

Overall, the heat transfer models and correlations discussed above provide a fairly complete methodology for determining the spray's key parameters of volumetric flux Q'' and Sauter mean diameter d_{32}, as well as the spatial distributions of these parameters based on nozzle inlet temperature and pressure drop, orifice diameter, cone angle, orientation angle, and orifice-to-surface distance. This information can be used to predict both cooling performance in the nucleate boiling region and CHF. One spray parameter that requires further study is the orifice-to-surface distance required to ensure fully developed droplet breakup prior to impact.

5 Hybrid High-Heat-Flux Cooling Schemes

As cooling demands challenge the capabilities of even the most promising mini/microchannel, jet, and spray cooling schemes, there is now a new focus on boosting thermal performance by combining key attributes of these schemes in the form of "hybrid" cooling schemes. Figure 13 shows one type of hybrid cooling that combines some of the advantages of both jet impingement and mini/microchannel cooling. Here the coolant is supplied into each of a number of parallel mini/microchannels either gradually, in the form of small circular jets, or as a single slot jet [51,52]. There are many possible variations of this hybrid configuration. For example, the jets supplying coolant to each channel could have equal diameters, or diameters that either increase or decrease from the centerline [53]. Supplying the coolant gradually with these hybrid schemes greatly decreases temperature gradients along the channels compared to conventional mini/microchannels, where the coolant is supplied from one end of the channel to the other
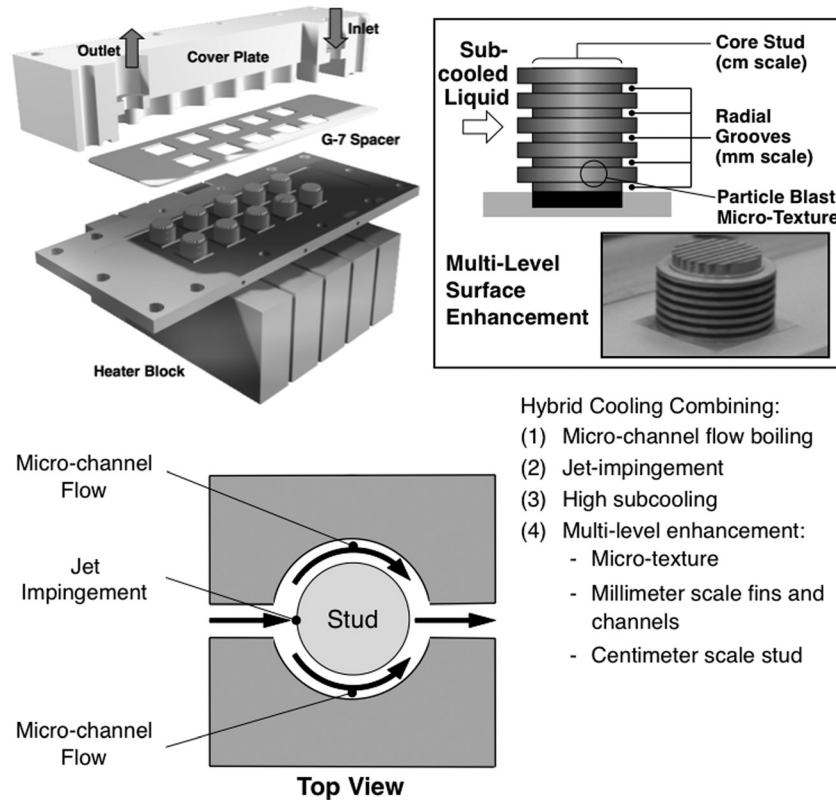
Fig. 14 Hybrid cooling scheme for very high-flux applications combining micro-channel flow, jet impingement, high subcooling, and multilevel surface enhancement (Meyer [54])

end. The gradual introduction of coolant suppresses the growth of void fraction along the channel, and therefore helps achieve higher CHF. The hybrid configurations also control the flow of spent jet fluid in individual channels, compared to uncontrolled flow in between impingement zones when using multiple conventional jets. Using HFE 7100 as coolant, this hybrid scheme proved capable of achieving an unprecedented heat flux of 1127 W/cm² without incurring CHF [53].

Figure 14 shows another example of hybrid cooling that combines benefits of (a) microchannel flow, (b) jet impingement, (c) highly subcooled boiling, and (d) surface enhancement to greatly increase CHF [54]. This configuration consists of a series of large studs, each attached to a heat dissipating device, with the coolant forced to first impinge along the front of the stud and afterwards flow in two parallel circumferential microchannels with the aid of a specially grooved cover plate. The stud itself combines three levels of surface enhancement: (a) centimeter-scale extended stud that contributes an appreciable increase in surface area in addition to the aforementioned control of coolant flow, (b) millimeter-scale grooves that contribute a further increase in surface area in addition to providing sharp corners that are highly favorable for bubble nucleation, and (c) microsurface texture (achieved by solid particle blasting or vapor blasting) to provide an abundance of surface cavities for efficient bubble nucleation. This hybrid cooling technique is an example of how standard cooling schemes can be combined advantageously to achieve superior cooling performance.

6 Conclusions

This study explored the implementation of two-phase mini/microchannel, jet, and spray cooling schemes into practical cooling packages, and the advantages and disadvantages of each scheme. The key focus of the study is assessment of available pre-dictive tools for cooling system design. Key findings from the study are as follows:

(1) Mini/microchannel cooling has received considerable attention in recent years, resulted in fairly comprehensive methods to predicting pressure drop, heat transfer coefficient, and CHF. Additional work is needed to predict conditions that trigger premature CHF and those that preclude its occurrence.

(2) Despite the attention two-phase jet-impingement cooling has received in recent years, no reliable correlations are available for the nucleate boiling region. There are sufficient tools to predict CHF for both confined circular jets and confined slot jets.

(3) A number of models and correlations are available that are crucial for spray cooling system design. These include tools to predict Sauter mean diameter d_{32} and the spatial distribution of volumetric flux Q'', based on nozzle pressure drop, orifice diameter, and cone angle. These parameters are then incorporated into available correlations to predict both nucleate boiling and CHF. Predictive tools are also available for the effects of nozzle orientation and overlap between spray impact areas when using multiple sprays. Further research is needed to investigate droplet breakup mechanisms and determine the orifice-to-surface distance required to ensure fully developed breakup.

(4) Overall, the design of cooling systems utilizing mini/microchannel, jet, or spray cooling schemes can benefit from consolidation of world databases for different coolants and broad ranges of operating conditions. Such efforts provide a systematic basis for recommending any necessary future experiments and developing reliable "universal" correlations for performance parameters of interest.

(5) The design of cooling systems can benefit from the development of efficient software tools and robust algorithms that are based on available models and correlations.

(6) Use of hybrid cooling schemes that combine the merits of mini/microchannel, jet, spray and other cooling schemes is a very effective means to achieving cooling performances unattainable with the individual cooling schemes.

Nomenclature

A = area measured along sprayed surface
A' = area measured along spherical surface centered at orifice of spray nozzle
Bo* = modified boiling number
C = empirical constant
c_p = specific heat at constant pressure
D = tube diameter
D_h = hydraulic diameter
d_j = jet diameter
d_o = diameter of spray nozzle's orifice
d_{32} = Sauter mean diameter (SMD) of spray
f = friction factor
f_1 = ratio of local to average volumetric flux of spray
f_2 = ratio of point-based CHF to CHF based on total area (L^2) of sprayed surface
G = mass velocity
g = gravitational acceleration
H = height; distance from spray or jet nozzle to surface
h = heat transfer coefficient
h_{fg} = latent heat of vaporization
k = thermal conductivity
L = tube length; axial span for boiling regime; length (and width) of jet impingement or spray surface
N = number of channels in heat sink
Nu = Nusselt number
P = pressure
ΔP = pressure drop across spray nozzle
Pr = Prandtl number
Q = total volumetric flow rate of spray
Q'' = local volumetric flux of spray on impact surface
$\overline{Q}''$ = mean volumetric flux across impact area of spray
q'' = heat flux based on total area (L^2) of sprayed surface
q''_m = critical heat flux
$q''_{m,p}$ = local (point-based) CHF at outer edge of spray impact area
q''_{**} = dimensionless CHF
r = radial distance measured from center of sprayed surface
Re = Reynolds number
Re_{d_0} = Reynolds number based on orifice diameter of spray nozzle
T = temperature
T_f = liquid temperature at inlet of spray nozzle
T_s = temperature of sprayed surface
T_w = temperature of channel wall
ΔT_{sub} = fluid inlet subcooling
U = jet velocity
U_m = mean droplet velocity of spray
v = specific volume
v_{fg} = specific volume difference between vapor and liquid
W = width; jet width
We = Weber number
We_{d_0} = Weber number based on orifice diameter of spray nozzle
x = x coordinate
X = Lockhart–Martinelli parameter
x_e = thermodynamic equilibrium quality
y = y coordinate

Greek Symbols

α = void fraction; inclination angle between spray axis and normal to surface
β = aspect ratio of rectangular channel; angle used in spray volumetric flux model

γ, γ' = angles used in uniform point source spray model
θ = spray cone angle
μ = viscosity
Π = dimensionless group
ρ = density
σ = surface tension
σ_c = contraction parameter
σ_e = expansion parameter
ϕ = two-phase multiplier

Subscripts

A = acceleration
c = contraction
ch = channel
d = downstream
dev = developing flow
e = expansion
f = liquid
F = friction
fo = liquid only
g = vapor
in = inlet
m = maximum (CHF)
max = maximum
min = minimum
ONB = onset of nucleate boiling
out = out
p = plenum; point-based (local)
s = sprayed surface
sat = saturated
sub = subcooled
tot = total
u = upstream
w = wall
1ϕ = one phase
2ϕ = two phase
3 = three-sided heated channel

References

[1] Anderson, T. M., and Mudawar, I., 1989, "Microelectronic Cooling by Enhanced Pool Boiling of a Dielectric Fluorocarbon Liquid," ASME J. Heat Transfer, **111**(3), pp. 752–759.
[2] Mudawar, I., 2011, "Two-Phase Microchannel Heat Sinks: Theory, Applications, and Limitations," ASME J. Electron. Packaging, **133**(4), p. 041002.
[3] Incropera, F., Dewitt, D., Bergman, T., and Lavine, A., 2007, *Fundamentals of Heat and Mass Transfer*, 6th ed., Wiley, Hoboken, NJ.
[4] Katto, Y., 1981, "General Features of CHF of Forced Convection Boiling in Uniformly Heated Rectangular Channels," Int. J. Heat Mass Transfer, **24**, pp. 1413–1419.
[5] Zuber, N., Tribus, M., and Westwater, J. W., 1961, "The Hydrodynamic Crisis in Pool Boiling of Saturated and Subcooled Liquids," Int. Dev. Heat Transfer: Proc. 1961–62, Int. Heat Transfer Conf., Boulder, CO, pp. 230–236.
[6] Galloway, J. E., and Mudawar, I, 1993, "CHF Mechanism in Flow Boiling From a Short Heated Wall—Part 1: Examination of Near-Wall Conditions With the Aid of Photomicrography and High-Speed Video Imaging," Int. J. Heat Mass Transfer, **36**, pp. 2511–2526.
[7] Galloway, J. E., and Mudawar, I, 1993, "CHF Mechanism in Flow Boiling From a Short Heated Wall—Part 2. Theoretical CHF Model," Int. J. Heat Mass Transfer, **36**, pp. 2527–2540.
[8] Nacke, R., Northcutt, B., and Mudawar, I., 2011, "Theory and Experimental Validation of Cross-Flow Micro-Channel Heat Exchanger Module With Reference to High Mach Aircraft Turbine Engines," Int. J. Heat Mass Transfer, **54**, pp. 1224–1235.
[9] Zhang, J., Fisher, T. S., Ramachandran, P. V., Gore, J., and Mudawar, I., 2005, "A Review of Thermal Issues in Hydrogen Storage Technologies," ASME J. Heat Transfer, **127**(12), pp. 1391–1399.
[10] Bowers, M. B., and Mudawar, I., 1994, "High Flux Boiling in Low Flow Rate, Low Pressure Drop Mini-Channel and Micro-Channel Heat Sinks," Int. J. Heat Mass Transfer, **37**, pp. 321–332.
[11] Bowers, M. B., and Mudawar, I., 1994, "Two-Phase Electronic Cooling Using Mini-Channel and Micro-Channel Heat Sinks—Part 1: Design Criteria and Heat Diffusion Constraints," ASME J. Electron. Packaging, **116**(4), pp. 290–297.
[12] Bowers, M. B., and Mudawar, I., 1994, "Two-Phase Electronic Cooling Using Mini-Channel and Micro-Channel Heat Sinks—Part 2: Flow Rate

and Pressure Drop Constraints," ASME J. Electron. Packaging, **116**(4), pp. 298–305.

[13] Bergles, A. E., 1977, "Review of Instability in Two-Phase Systems," *Two-Phase Flows and Heat Transfer*, Vol. 1, S. Kakac, and F. Mayinger, eds., Hemisphere, Washington, pp. 383–422.

[14] Yadigaroglu, G., 1981, "Two-Phase Flow Instabilities and Propagation Phenomena," *Thermohydraulics of Two-Phase Systems for Industrial Design and Nuclear Engineering*, J. M. Delhaye, M. Giot, and M. L. Riethmuller, eds., Hemisphere, Washington, DC, pp. 353–403.

[15] Qu, W., and Mudawar, I., 2003, "Measurement and Prediction of Pressure Drop in Two-Phase Micro-Channel Heat Sinks," Int. J. Heat Mass Transfer, **46**, pp. 2737–2753.

[16] Lee, J., and Mudawar, I., 2008, "Fluid Flow and Heat Transfer Characteristics of Low Temperature Two-Phase Micro-Channel Heat Sinks—Part 2: Subcooled Boiling Pressure Drop and Heat Transfer," Int. J. Heat Mass Transfer, **51**, pp. 4327–4341.

[17] Lockhart, R. W., and Martinelli, R. C., 1949, "Proposed Correlation of Data for Isothermal Two-Phase, Two-Component Flow in Pipes," Chem. Eng. Progress, **45**, pp. 39–48.

[18] Lee, J., and Mudawar, I., 2005, "Two-Phase Flow in High-Heat-Flux Micro-Channel Heat Sink for Refrigeration Cooling Applications: Part I—Pressure Drop Characteristics," Int. J. Heat Mass Transfer, **48**, pp. 928–940.

[19] Shah, R. K., and London, A. L., 1978, *Laminar Flow Forced Convection in Ducts: A Source Book for Compact Heat Exchanger Analytical Data*, Academic, New York, Suppl. 1.

[20] Qu, W., and Mudawar, I., 2002, "Prediction and Measurement of Incipient Boiling Heat Flux in Micro-Channel Heat Sinks," Int. J. Heat Mass Transfer, **45**, pp. 3933–3945.

[21] Sato, T., and Matsumura, H., 1963, "On the Conditions of Incipient Subcooled Boiling and Forced-Convection," Bull. JSME, **7**, pp. 392–398.

[22] Kim, S. M., and Mudawar, I., 2012, "Consolidated Method to Predicting Pressure Drop and Heat Transfer Coefficient for Both Subcooled and Saturated Flow Boiling in Micro-Channel Heat Sinks," Int. J. Heat Mass Transfer, **55**, pp. 3720–3731.

[23] Lee, J., and Mudawar, I., 2009, "Critical Heat Flux for Subcooled Flow Boiling in Micro-Channel Heat Sinks," Int. J. Heat Mass Transfer, **52**, pp. 3341–3352.

[24] Hall, D. D., and Mudawar, I., 1999, "Ultra-High Critical Heat Flux (CHF) for Subcooled Water Flow Boiling—II. High-CHF Database and Design Parameters," Int. J. Heat Mass Transfer, **42**, pp. 1429–1456.

[25] Mudawar, I., and Bowers, M. B., 1999, "Ultra-High Critical Heat Flux (CHF) for Subcooled Water Flow Boiling—I. CHF Data and Parametric Effects for Small Diameter Tubes," Int. J. Heat Mass Transfer, **42**, pp. 1405–1428.

[26] Katto, Y., and Monde, M., 1974, "Study of Mechanism of Burnout in High Heat Flux Boiling Systems With an Impinging Jet," Proc. 5th Int. Heat Transfer Conf., Tokyo, Japan, Paper No B6.2, pp. 245–249.

[27] Monde, M., and Katto, Y., 1978, "Burnout in High Heat-Flux Boiling System With an Impinging Jet," Int. J. Heat Mass Transfer, **21**, pp. 295–305.

[28] Katto, Y., and Ishii, K., 1978, "Burnout in a High Heat Flux Boiling System With a Forced Supply of Liquid Through a Plane Jet," Proc. 6th Int. Heat Transfer Conf., Toronto, Canada, Vol. 1, pp. 435–440.

[29] Monde, M., 1987, "Critical Heat Flux in Saturated Forced Convection Boiling on a Heated Disk With an Impinging Jet," ASME J. Heat Transfer, **109**(4), pp. 991–996.

[30] Monde, M., and Inoue, T., 1991, "Critical Heat Flux in Saturated Forced Convective Boiling on a Heated Disk With Multiple Impinging Jets," ASME J. Heat Transfer, **113**(3), pp. 722–727.

[31] Katto, Y., and Shimizu, M., 1979, "Upper Limit of CHF in the Saturated Forced Convection Boiling on a Heated Disk With a Small Impinging Jet," ASME J. Heat Transfer, **101**(2), pp. 265–269.

[32] Estes, K. A., and Mudawar, I., 1995, "Comparison of Two-Phase Electronic Cooling Using Free Jets and Sprays," ASME J. Electron. Packaging, **117**(4), pp. 323–332.

[33] Mudawar, I., and Wadsworth, D. C., 1991, "Critical Heat Flux From a Simulated Chip to a Confined Rectangular Impinging Jet of Dielectric Liquid," Int. J. Heat Mass Transfer, **34**, pp. 1465–1479.

[34] Johns, M. E., and Mudawar, I., 1996, "An Ultra-High Power Two-Phase Jet-Impingement Avionic Clamshell Module," ASME J. Electron. Packaging, **118**(4), pp. 264–270.

[35] Meyer, M. T., Mudawar, I., Boyack, C. E., and Hale, C. A., 2006, "Single-Phase and Two-Phase Cooling With an Array of Rectangular Jets," Int. J. Heat Mass Transfer, **49**, pp. 17–29.

[36] Wadsworth, D. C., and Mudawar, I., 1992, "Enhancement of Single-Phase Heat Transfer and Critical Heat Flux From an Ultra-High-Flux Simulated Microelectronic Heat Source to a Rectangular Impinging Jet of Dielectric Liquid," ASME J. Heat Transfer, **114**(3), pp. 764–768.

[37] Mudawar, I., and Valentine, W. S., 1989, "Determination of the Local Quench Curve for Spray-Cooled Metallic Surfaces," J. Heat Treating, **7**, pp. 107–121.

[38] Toda, S., 1972, "A Study in Mist Cooling (1st Report: Investigation of Mist Cooling)," Trans. JSME, **38**, pp. 581–588.

[39] Monde, M., 1980, "Critical Heat Flux in Saturated Forced Convection Boiling With an Impinging Droplet," Trans. JSME, **46**, pp. 1146–1155.

[40] Ghodbane, M., and Holman, J. P., 1991, "Experimental Study of Spray Cooling With Freon-113," Int. J. Heat Mass Transfer, **34**, pp. 1163–1174.

[41] Holman, J. P., and Kendall, C. M., 1993, "Extended Studies of Spray Cooling With Freon-113," Int. J. Heat Mass Transfer, **36**, pp. 2239–2241.

[42] Rini, D. P., Chen, R.-H., and Chow, L. C., 2002, "Bubble Behavior and Nucleate Boiling Heat Transfer in Saturated FC-72 Spray Cooling," ASME J. Heat Transfer, **124**(1), pp. 63–72.

[43] Cho, C. S. K., and Wu, K., 1988, "Comparison of Burnout Characteristics in Jet Impingement Cooling and Spray Cooling," Proc. National Heat Transfer Conf., Houston, TX, pp. 561–567.

[44] Chen, R.-H., Chow, L. C., and Navedo, J. E., 2002, "Effects of Spray Characteristics on Critical Heat Flux in Subcooled Water Spray Cooling," Int. J. Heat Mass Transfer, **45**, pp. 4033–4043.

[45] Lin, L., and Ponnappan, R., 2003, "Heat Transfer Characteristics of Spray Cooling in a Closed Loop," Int. J. Heat Mass Transfer, **46**, pp. 3737–3746.

[46] Hall, D. D., and Mudawar, I., 1995, "Experimental and Numerical Study of Quenching Complex-Shaped Metallic Alloys With Multiple, Overlapping Sprays," Int. J. Heat Mass Transfer, **38**, pp. 1201–1216.

[47] Estes, K. A., and Mudawar, I., 1995, "Correlation of Sauter Mean Diameter and Critical Heat Flux for Spray Cooling of Small Surfaces," Int. J. Heat Mass Transfer, **38**, pp. 2985–2996.

[48] Mudawar, I., and Estes, K. A., 1996, "Optimizing and Predicting CHF in Spray Cooling of a Square Surface," ASME J. Heat Transfer, **118**(3), pp. 672–679.

[49] Rybicki, J. R., and Mudawar, I., 2006, "Single-Phase and Two-Phase Cooling Characteristics of Upward-Facing and Downward-Facing Sprays," Int. J. Heat Mass Transfer, **49**, pp. 5–16.

[50] Visaria, M., and Mudawar, I., 2009, "Application of Two-Phase Spray Cooling for Thermal Management of Electronic Devices," IEEE Trans. Comp. Pack. Technol., **32**, pp. 784–793.

[51] Sung, M. K., and Mudawar, I., 2008, "Single-Phase and Two-Phase Heat Transfer Characteristics of Low Temperature Hybrid Micro-Channel/Micro-Jet Impingement Cooling Module," Int. J. Heat Mass Transfer, **51**, pp. 3882–3895.

[52] Sung, M. K., and Mudawar, I., 2009, "Effects of Jet Pattern on Two-Phase Cooling Performance of Hybrid Micro-Channel/Micro-Circular-Jet-Impingement Thermal Management Scheme," Int. J. Heat Mass Transfer, **52**, pp. 3364–3372.

[53] Sung, M. K., and Mudawar, I., 2009, "Single-Phase and Two-Phase Hybrid Cooling Schemes for High-Heat-Flux Thermal Management of Defense Electronics," ASME J. Electron. Packaging, **131**(2), p. 021013.

[54] Meyer, M., 2006, "Apparatus for Heat Transfer and Critical Heat Flux Enhancement," U.S. Patent No. 7,035,104.